Adsorption of Ethyl Benzene on Activated Carbon from Supercritical CO_2

R. Harikrishnan, M. P. Srinivasan, and C. B. Ching
Dept. of Chemical Engineering, National University of Singapore, Singapore, 119260

Our work involves experimental and simulation studies of the adsorption breakthrough and equilibria of ethyl benzene (a pollutant commonly encountered in industrial waste streams) on activated carbon in the presence of supercritical carbon dioxide. Frontal and single breakthrough saturations were analyzed for a range of operating conditions of pressure (100 – 130 bar) and temperature (313 – 338 K). The equilibrium data correlated well with the Langmuir isotherm. The adsorption process was successfully modeled by a three-parameter model with comparable fitting parameters for the two types of breakthrough curves.

Introduction

The adsorption ability of porous solids is a property that has many applications in large-scale separation and purification processes. Activated carbons are processed carbon material that are capable of adsorbing various substances from gas and liquid streams because of their highly developed pore structure and large internal specific surface areas. The applications of these materials include solvent recovery processes, adsorption from waste streams, vacuum technology, adsorption gas chromatography, catalyst supports, and electrode material in electrochemistry.

The increasing awareness of the necessity for environmental safety and pollution control has opened new prospects for activated carbons. In many industrial processes such as printing, coating, textile dyeing, spray painting, and polymer processing, emission of volatile organic compounds (VOCs) is a major economic and environmental concern. Some of the common VOCs that are perceived as environmental hazards are chloroalkanes, benzene, toluene and their derivatives, xylenes, chloroform, and glycol ethers. Activated carbon adsorption is one of the most effective methods of recovering these solvents from a variety of process streams. After the exhaustion of their full adsorption capacities, these carbons have been subjected to treatment not only to recover the solvents, but also to reuse the carbon material for further adsorption.

The application of supercritical fluids has expanded from extraction, adsorption and desorption processes, and chromatography to polymer engineering and supercritical fluid coatings during the past two decades. For a fluid to have wide applications as an extraction solvent or a mobile phase for chromatography, it is essential for it to possess significant solvating strength. The solvent power of a fluid is directly related to its solvent density. When supercritical fluids are compressed, they exhibit liquid-like densities and thereby possess enhanced solvation characteristics. This is evident from the fact that, when intermolecular distances in a fluid are reduced, the molecular interactions are enhanced, thus leading to greater solvating power. Furthermore, in the vicinity of the fluid critical point, that is, $0.9 \leq T_r \leq 1.2$ and $0.7 \leq P_r \leq 1.1$, the supercritical fluid density increases significantly from low values to those comparable with liquid-like densities. Supercritical fluids also possess favorable physicochemical properties such as diffusivities and viscosities in between those of liquids and gases. The combination of enhanced solvent properties and mass-transfer characteristics makes supercritical fluid extractions extremely advantageous compared with conventional solvent extractions. Of the various solvents available, carbon dioxide has been used extensively because of its inert, nontoxic, and noninflammable nature; low cost; easy availability; and favorable critical temperature of about 304 K, which is close to ambient conditions.

Scope of Work

The primary aim of our work is to study the dynamics of the adsorption–desorption process involving solutes that are strongly adsorbed on the adsorbent in the presence of supercritical CO_2. To accomplish this, detailed study of the solute's adsorption equilibria in the presence of the supercritical fluid phase is essential. Various researchers such as Kander and

Correspondence concerning this article should be addressed to M. P. Srinivasan.

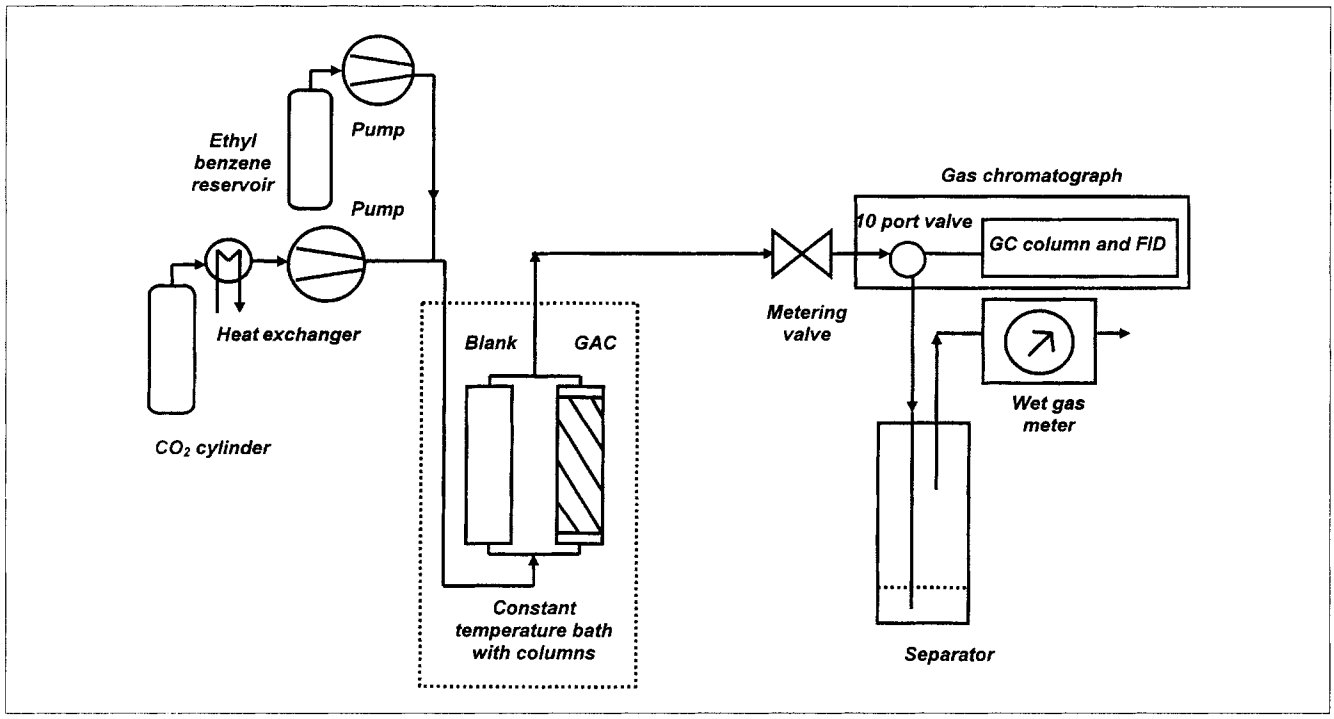

Figure 1. Laboratory-scale experimental setup for supercritical adsorption studies.

Paulaitis (1983), Erkey et al. (1993), Macnaughton and Foster (1995), and Shojibara et al. (1995) have investigated the equilibrium phenomenon employing different solutes. But the range of solutes industrially classified as VOCs is extensive. This, in addition to the fact that VOCs adsorb with various degrees of strength, necessitates exploration of a variety of solutes to arrive at a general proposition for sorption equilibrium phenomena of organics under these conditions. In our work, we have considered ethyl benzene as a potential VOC and have extensively studied the experimental as well as modeling aspects of the adsorption equilibria over activated carbon in the presence of supercritical CO_2.

Experimental Studies

The experimental apparatus employed for the study is shown in Figure 1. Virgin activated carbon (BDH; charcoal granular activated; particle size 10–18 mesh) was packed in a stainless steel tube with stainless steel frits (Supelco) on either side to confine the carbon to the column. A systematic procedure was adopted before packing the carbon to prepare it for experimental purposes. The virgin carbon was initially screened to obtain an 18–20 mesh fraction (average particle size is 0.001 m) and then boiled in deionized water repeatedly to remove the fines. The sample was dried in an oven at about 423 K in the presence of an inert atmosphere of purified nitrogen (Soxal, 99.9995%). About 0.025 kg of this prepared carbon was packed in the column to constitute a fixed bed. Properties of the packed bed are shown in Table 1. In order to neutralize the column end effects on the experimental observations, an identical column packed with spherical glass beads (0.001-m dia.) was placed parallel with the granular activated carbon (GAC) column. The two columns were immersed in an insulated constant temperature bath. The temperature was controlled by an immersion circulator (Polyscience; model 9101) with an average temperature stability of about 0.01°C. A coil positioned in front of the column in the constant temperature bath ensured that the fluid reached the bath temperature before entering the bed. Preliminary experiments were conducted to confirm this.

Purified CO_2 (Soxal, 99.8%) was sent into the fixed bed by an HPLC pump (LC-9A Shimadzu liquid chromatograph). The other HPLC pump (HP series 1050) was used to pump the pollutant (ethyl benzene) into the fixed bed as shown in Figure 1. The exit concentrations of the solutes in the supercritical phase were monitored using a gas chromatograph (Perkin Elmer Autosystem XL) by employing flame ionization method as the detection technique. The fluid was chilled at the exit of the gas chromatograph (GC) by a refrigerated circulating bath (NESLAB Endocal) so as to collect the solutes in an ethanol-water mixture and the carbon dioxide was discharged as exhaust. The CO_2 flow rates were measured by a wet gas meter (Sinagawa; W-NK model 1A) at the exit conditions. In order to confirm the trace of the concentration profiles, preliminary experiments were conducted using an online SPD-6A Shimadzu UV spectrophotometer that recorded the absorbance profiles on a recorder (Rikadenki multi-pen recorder). The calibration graph between ab-

Table 1. Properties of Packed Bed

Length of packed bed, L	0.302 m
OD of column, D	0.019 m
Porosity of bed, ϵ	0.38
Particle density, ρ_p	800.8 kg/m^3
Particle porosity, α	0.535
Particle radius, r_p	0.0005 m
Specific surface area	1,316 m^2/g

sorbance and concentration generated from preliminary experiments was used to determine the exit concentration profile.

Experimental Procedure

The experimental procedure primarily involved an adsorption and a desorption step. During the adsorption process, ethyl benzene was adsorbed on the active carbon by a frontal analysis technique. In this method, the fluid phase concentration of ethyl benzene was increased in sequential steps and adsorption equilibrium was established on exposure of the carbon surface to each concentration level until the adsorption capacity was reached. Initially, supercritical CO_2 was pumped through the blank column packed with glass beads to establish a baseline for pure CO_2 flowing through the GC. A known concentration of ethyl benzene was then introduced through the HPLC pump to obtain the saturation concentration chromatogram. Equal-area chromatograms from successive samplings indicated that a uniform ethyl benzene concentration pervaded through the fluid phase of the blank column. The flow was then switched to the GAC column in order to commence the adsorption process. It was possible to view the status of the adsorption breakthrough from the output of the GC. The GC was calibrated using a range of concentrations and the calibration plot between the chromatogram area and ethyl benzene concentration in carbon dioxide was used to determine the trace of the breakthrough. The concentration of ethyl benzene in the fluid stream was increased to begin the second step of the frontal adsorption breakthrough after equilibrium was reached for the first step.

Mathematical model development for frontal breakthrough Analysis

Mathematical modeling of adsorption breakthrough curves has been studied quite extensively. Ruthven (1984) did a comprehensive compilation of models for both linear and nonlinear systems. Tan and Liou (1988), Recasens et al. (1989), and Reverchon (1997) have simulated the desorption efficiency curves. Porto Jefferson et al. (1995) investigated the effect of intraparticle diffusion and external mass transfer on the dynamics of benzene adsorption on activated carbon in supercritical CO_2. While greater attention has been diverted to single breakthrough analysis or desorption modeling, we have concentrated on the adsorption modeling of the frontal breakthrough under supercritical conditions. To our knowledge, this is the first time that modeling of an entire frontal sequence has been attempted at supercritical conditions.

The model was developed considering the following assumptions:

1. Isothermal adsorption occurs.
2. Axial dispersion (valid assumption for supercritical fluids; Recasens et al., 1989) is negligible.
3. Mass transport from bulk fluid phase to the fluid inside the particle occurs through a film; the resistance is characterized by a transfer coefficient k_f.
4. Concentration of solute inside the particle C_i is averaged over the volume of the solid particle to yield $\overline{C_p}$, where

$$\overline{C_p} = \frac{3}{r_p^2}\int_0^{r_p} C_i(r) r^2 dr \tag{1}$$

5. A transfer resistance represented as k_p, which includes the external film and intraparticle diffusion effects, governs the gradient between the fluid concentration and the average pore concentration of the solute. Hypothesizing a parabolic concentration profile inside the pore as suggested by Do and Rice (1986), k_p can be evaluated from k_f and D_p.

$$\frac{1}{k_p} = \frac{1}{k_f} + \frac{r_p}{5D_p} \tag{2}$$

6. The solid-phase mass-transfer coefficient k_s and the surface driving force determine the rate at which the instantaneous surface loading approaches the equilibrium loading.

Considering the mass balances in three different control volumes, the fluid phase in the columns external and internal to the particle, and the solid surface of the particle, the proposed model is governed by the following differential equations:

$$\epsilon\frac{\partial C_f}{\partial t} + u\frac{\partial C_f}{\partial z} + \frac{3(1-\epsilon)k_p}{r_p}\left(C_f - \overline{C_p}\right) = 0 \tag{3}$$

$$a\frac{\partial \overline{C_p}}{\partial t} = \frac{3k_p}{r_p}\left(C_f - \overline{C_p}\right) - \rho\frac{\partial \bar{q}}{\partial t} \tag{4}$$

$$\frac{\partial \bar{q}}{\partial t} = k_s(q^* - \bar{q}) \tag{5}$$

The equilibrium relationship is modeled using the Langmuir adsorption isotherm.

$$q^* = \frac{q_s b\overline{C_p}}{1 + b\overline{C_p}} \tag{6}$$

The initial and boundary conditions that define the model are given by

$$C_f(z > 0, t = 0) = C_{fo} \tag{7}$$

$$\overline{C_p}(z > 0, t = 0) = \overline{C}_{po} \tag{8}$$

$$\bar{q}(z > 0, t = 0) = \bar{q}_o \tag{9}$$

$$C_f(z = 0, t > 0) = C_{fi} \tag{10}$$

The numerical values vary for each of the initial and boundary conditions and correspond to the particular step under investigation in the frontal analysis. Rewriting the model equations in dimensionless format, the boundary value problem (BVP) was transformed into an initial value problem (IVP) using the orthogonal collocation method suggested by Villadsen et al. (1978). A minimum of 13 collocation points for convergence were used to solve the equations. In order to achieve greater accuracy, the results were generated using 16 collocation points. Program run times were found to be insignificant.

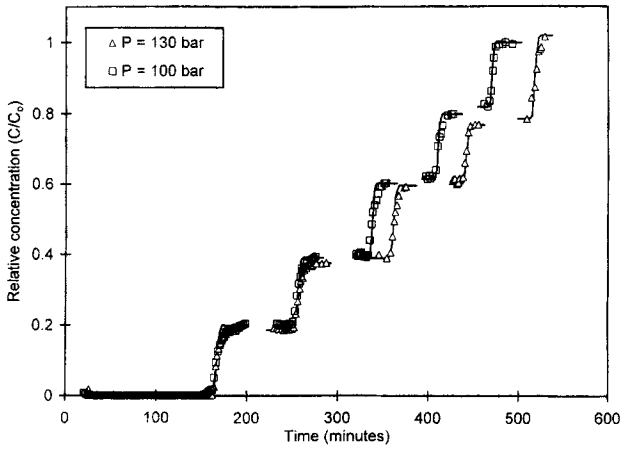

Figure 2. Experimental and simulated frontal breakthrough curves at 318 K.

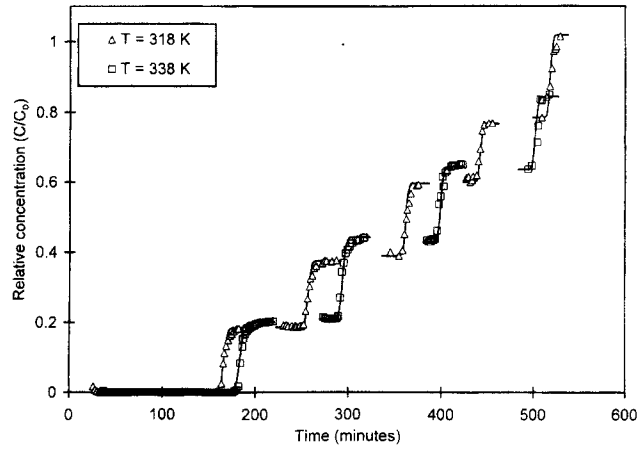

Figure 3. Experimental and simulated frontal breakthrough curves at 130 bar.

Results and Discussion

Analysis of breakthrough curves

The adsorption breakthrough curves for ethyl benzene were generated experimentally by the frontal chromatography technique in which the supercritical fluid phase was subjected to sequential increments in solute concentrations of ethyl benzene and the exit concentrations were monitored. From the breakthrough curves, the respective ethyl benzene loadings on GAC were determined for different inlet concentrations of the fluid phase. An important observation was the saturation of a significantly large portion of the absorbent capacity at the lowest fluid-phase concentration of ethyl benzene. This may be due to the initial filling of the most active sites of the adsorbent that contribute significantly to the adsorption capacity. As the ethyl benzene concentration in the fluid phase was increased to obtain successive frontal breakthrough curves, the available sites for adsorption decreased, resulting in reduced adsorption in comparison with the previous frontal steps. Experimental results were obtained for various combinations of temperature (313–338 K) and pressure (100–130 bar) as shown in Figures 2 and 3 (marked symbols represent experimental results). Since each frontal step yielded a single point on the adsorption isotherm curves, a complete set of equilibrium data was obtained for the ethyl benzene-SC CO_2- GAC system.

Analysis of isotherm data

Adsorption experimental data obtained for ethyl benzene over the range of operating conditions of temperature and pressure were fitted to Langmuir adsorption isotherms. The fitting parameters for the isotherms were determined from the Langmuir plots as shown in Figure 4. The parameter values are shown in Table 2.

The shape of the curves indicated the favorable nature of the adsorption isotherms. The limitations of the experimental conditions employing supercritical fluids restricted the data generation to the nonlinear region of the isotherm. The effects of operating parameters, temperature and pressure, and fluid properties such as solubility and density on solute loading were studied to derive relevant information from the adsorption data.

The salient observations are summarized below:

1. Increasing the operating pressure of adsorption under isothermal conditions resulted in a decrease in equilibrium adsorption loading (Figure 5). Shojibara et al. (1995) observed a similar phenomenon for benzene adsorption on activated carbon under supercritical conditions. This effect seemed to be more pronounced at temperatures closer to the fluid critical temperature due to higher solute solubility at elevated supercritical pressures.

2. The influence of pressure on loading weakened, further away from T_c in the supercritical region, as shown in Figure 6. This suggested the existence of a transition temperature (in the range 328–338 K) below which the supercritical phase solubility effect appeared dominant.

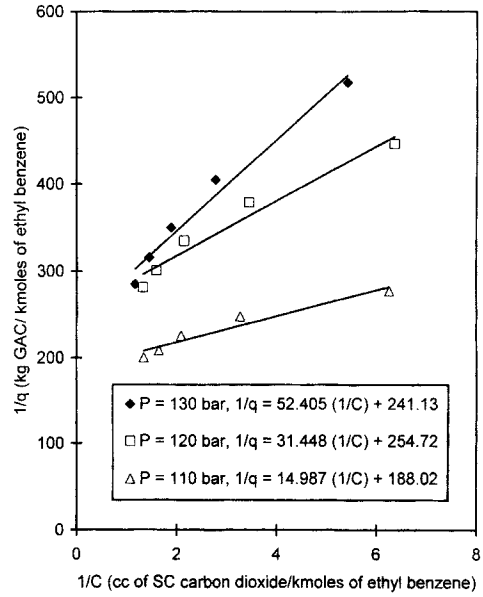

Figure 4. Langmuir plot at 313 K.

Table 2. Langmuir Isotherm Parameters for Adsorption of Ethyl Benzene on GAC in the Presence of SC CO_2

Temp.	313 K		318 K		328 K		338 K	
Pres (bar)	q_s (kmol/kg)	b (m^3/kmol)	q_s (kmol/kg)	b (m^3/kmol)	q_s (kmol/kg)	b (m^3/kmol)	q_s (kmol/kg)	b (m^3/kmol)
100	0.0046	9.99	0.004	14.60	0.0039	35.15	—	—
110	0.0053	12.55	0.0043	10.16	0.0030	16.13	0.0036	31.61
120	0.0039	8.09	0.0034	13.56	0.0032	19.74	0.0035	26.25
130	0.0041	4.60	0.0039	7.99	0.0047	11.87	0.0040	17.14

3. Under isobaric conditions closer to the fluid critical pressure P_c, the loading decreased with an increase in temperature (Figures 5 and 7). This sorption phenomenon was due to the temperature effect on loading.

4. At pressures about 120 bar (Figure 8), restricted variation in solubility in the temperature range 318–328 K resulted in invariant loading. However, at higher supercritical temperatures (338 K), lower solubility resulted in higher loading. The transition behavior of solute solubility in the supercritical phase with respect to temperature can be visualized in the solubility plot for naphthalene in supercritical carbon dioxide (Kander and Paulaitis, 1983). Tan and Liou (1988) and Recasens et al. (1989) also observed this trend and our observations support their investigations. Chimowitz and Pennisi (1986) examined these unusual phenomena as a crossover effect and have indicated that the phenomena result from the effect of temperature on density at elevated pressures. Thus, a region of transition may exist (120–130 bar) where control over the influence on loading shifts from temperature to solubility.

5. At a higher pressure of 130 bar, which falls in the transition region in the solubility plot of naphthalene (120–150 bar), our investigations showed an increase in loading with temperature (Figure 9), which is similar to the effect of decreasing solubility on loading at 120 bar and 338 K. Though solubility variation was not clear from the naphthalene solubility plot (Kander and Paulaitis, 1983), our observations further support the earlier contention (point 4) that a transition region exists for indicating the controlling factor on loading.

Modeling the breakthrough curves

To obtain best matches for the experimental breakthrough curves the film, pore, and surface mass-transfer resistances were independently taken into consideration, as opposed to using an overall resistance model. The steep nature of the breakthrough curves suggested negligible influence of axial dispersion effects on loading. The modeling procedure involved the estimation of parameters like k_f, D_f, k_p, D_p, and k_s. The starting value of k_f was determined from the correlation (Wakao and Kaguei, 1982)

$$\frac{2k_f r_p}{D_f} = 2 + 1.1(Re)^{0.6}(Sc)^{1/3} \tag{11}$$

where Re and Sc represent the Reynolds and Schmidt numbers.

$$Re = \frac{2u\rho r_p}{\mu} \tag{12}$$

$$Sc = \frac{\mu}{\rho D_f} \tag{13}$$

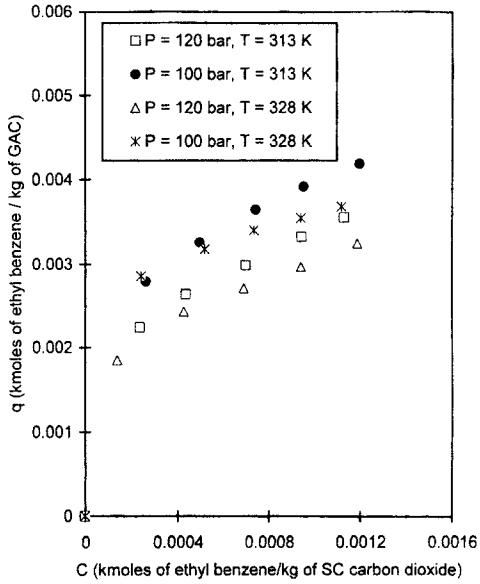

Figure 5. Adsorption equilibria at: 313 K vs. 328 K.

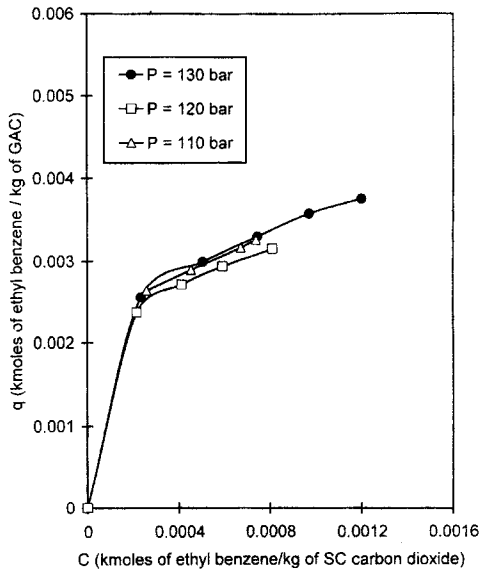

Figure 6. Adsorption equilibrium at 338 K.

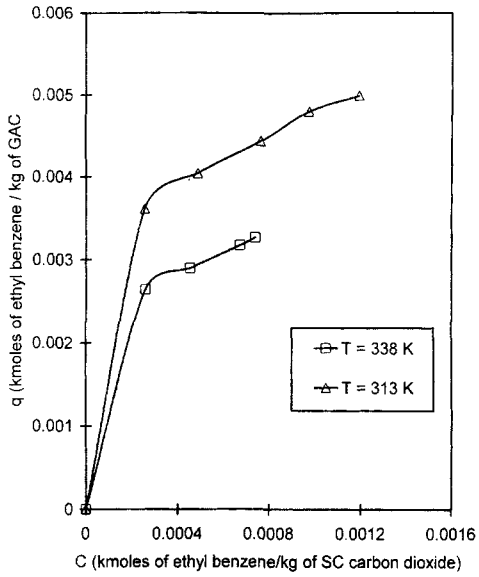

Figure 7. Comparison of adsorption equilibria at 110 bar.

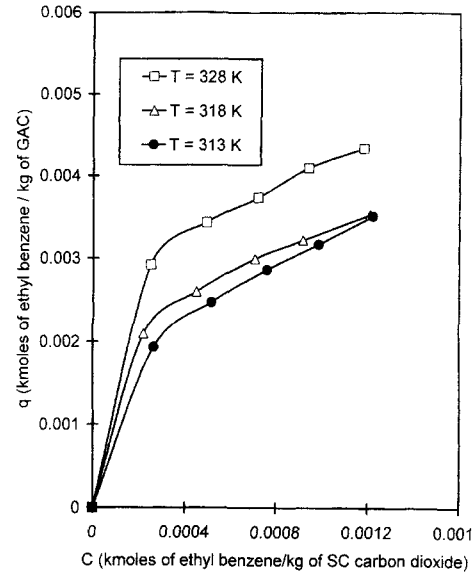

Figure 9. Adsorption equilibrium at 130 bar.

The estimation of D_f was by Takahashi's correlation (Reid et al., 1987), which relates the product $D_{AB}P$ at elevated pressures to products at lower pressures, $(D_{AB}P)^*$ through a function $f(T_r, P_r)$ in the form

$$\frac{D_{AB}P}{(D_{AB}P)^*} = f(T_r, P_r) \tag{14}$$

Density and viscosity of the fluid at the various operating conditions were estimated from established correlations documented in Reid et al. (1987). The starting value for the parameter D_p was predicted by assuming a value of $1/\alpha$ for the tortuosity factor τ. The validity of this assumption was based on τ being a geometric factor independent of temperature or nature of the diffusing species and inversely proportional to the particle porosity α.

The simulated results (shown as continuous curves in Figures 2 and 3) gave the optimized fitted values for k_f, D_p, and k_s. Employing the linear driving force model relating D_p and k_p, the optimum values for k_p were also obtained. The tortuosity factors for the adsorbent were calculated using the relation between the predicted D_f and the fitted D_p values and an average value of four was obtained.

$$\tau = \alpha \frac{D_f}{D_p} \tag{15}$$

Fitting all experimental breakthrough curves with reasonable accuracy necessitated considering a significant solid film resistance, measured by k_s, which is related approximately to the solid diffusion coefficient D_s and the solid film thickness δ_f by

$$\delta_f = \frac{D_s}{k_s} \tag{16}$$

A typical characteristic of a nonlinear adsorption relationship such as the Langmuir isotherm is the variation in bond energy with loading resulting in a concentration-dependent surface diffusivity. Although several investigators, such as Neretnieks (1976) and Seidel and Carl (1989), have derived equations for depicting the concentration dependence of D_s, no confirmed general theories currently exist to explain the dependence phenomena. Extending the same principle to surface mass transport, we expect k_s to be a function of concentration. It is impractical, however, to measure the influence of surface resistance on loading by distinctly neglecting the other transfer interferences under these experimental conditions. Even if an exponential relationship or an adsorption isotherm-based equation was assumed to fit the experimental data, the functional dependence is not necessarily proven accurate. As a result, an adequate assumption that

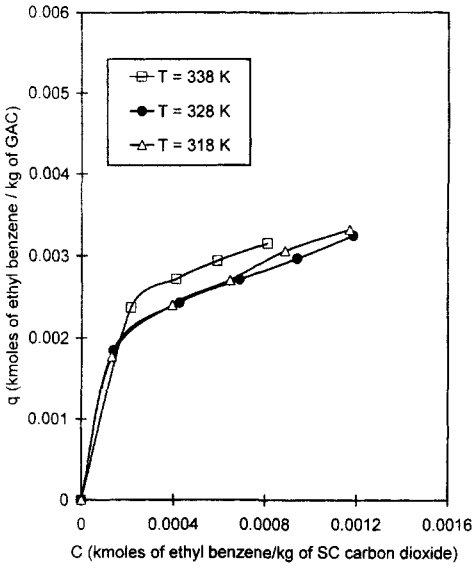

Figure 8. Adsorption equilibrium at 120 bar.

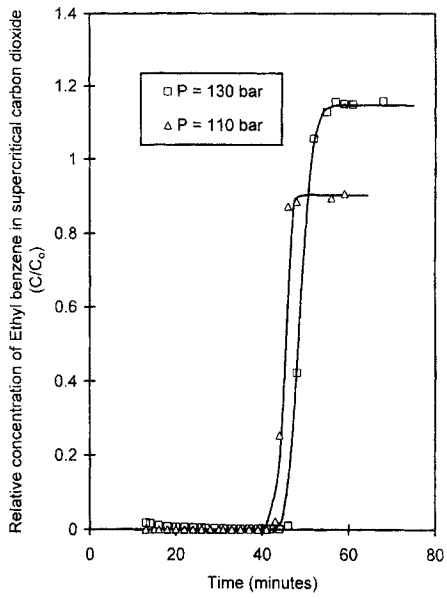

Figure 10. Experimental and simulated single breakthrough at 338 K.

was sufficient to fit all experimental breakthroughs was to consider k_s as a constant fitting parameter. An average value of 1.567×10^{-7} m/s was obtained for k_s.

Although our assumption pertaining to the surface mass transport was not completely realistic, it does give an opportunity to simplify the effect of taking an additional resistance into account. As mentioned earlier, the overall transport of the ethyl benzene from the fluid phase to the adsorbent surface is controlled by three resistance mechanisms. Assuming one of these resistance parameters k_s to be constant does

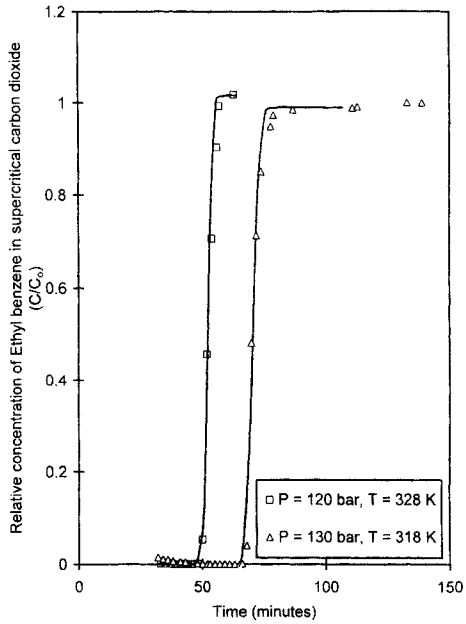

Figure 11. Experimental and simulated single breakthrough at 328 K and 120 bar; 318 K and 130 bar.

Table 3. Modeling Parameters for Frontal Breakthrough Curves

Temp. (K)	Pres. (bar)	k_f	D_p
338	130	6.393×10^{-5}	9.941×10^{-10}
		3.608×10^{-5}	9.941×10^{-10}
		2.261×10^{-5}	9.941×10^{-10}
		2.261×10^{-5}	9.941×10^{-10}
		0.926×10^{-5}	9.941×10^{-10}
338	120	3.754×10^{-4}	3.907×10^{-9}
		1.684×10^{-4}	3.907×10^{-9}
		9.784×10^{-5}	3.907×10^{-9}
		5.400×10^{-5}	3.907×10^{-9}
		4.140×10^{-5}	3.907×10^{-9}
328	130	1.610×10^{-4}	2.835×10^{-9}
		9.894×10^{-5}	2.835×10^{-9}
		4.554×10^{-5}	2.835×10^{-9}
		4.054×10^{-5}	2.835×10^{-9}
		3.054×10^{-5}	2.835×10^{-9}
328	110	2.770×10^{-4}	3.898×10^{-9}
		9.970×10^{-5}	3.898×10^{-9}
		7.970×10^{-5}	3.898×10^{-9}
		6.970×10^{-5}	3.898×10^{-9}
		5.840×10^{-5}	3.898×10^{-9}
328	100	4.535×10^{-4}	4.399×10^{-9}
		1.233×10^{-4}	4.399×10^{-9}
		9.233×10^{-5}	4.399×10^{-9}
		5.535×10^{-5}	4.399×10^{-9}
		5.535×10^{-5}	4.399×10^{-9}
318	130	1.109×10^{-4}	2.155×10^{-9}
		6.309×10^{-4}	2.155×10^{-9}
		3.409×10^{-5}	2.155×10^{-9}
		1.403×10^{-5}	2.155×10^{-9}
		1.403×10^{-5}	2.155×10^{-9}
318	110	1.825×10^{-4}	2.792×10^{-9}
		9.680×10^{-5}	2.792×10^{-9}
		5.480×10^{-5}	2.792×10^{-9}
		3.682×10^{-5}	2.792×10^{-9}
		2.680×10^{-5}	2.792×10^{-9}
318	100	2.683×10^{-4}	3.314×10^{-9}
		1.170×10^{-4}	3.314×10^{-9}
		8.117×10^{-5}	3.314×10^{-9}
		5.117×10^{-5}	3.314×10^{-9}
		4.117×10^{-5}	3.314×10^{-9}

For successive steps of the frontal breakthrough.

cause the range of other fitting parameters k_f and D_p to conform to those of the predicted values.

This approach was also confirmed when excellent fits, shown in Figures 10 and 11, were obtained for the experimental single breakthrough curves from a different set of experiments. The entire set of single breakthrough parameters was in close agreement with those simulated for the sequential frontal curves for the same experimental conditions. All the modeling results are presented in Tables 3 and 4. The optimized parameter values obtained for k_f, k_p, D_f, D_p, and τ agreed well with previously published results by Recasens et al. (1989). In our study, the excellent match between the experimental and the model predictions confirmed the ability of the three-parameter model to successfully describe the dynamics of ethyl benzene adsorption on a fixed bed of GAC within the wide range of the operating conditions investigated.

Table 4. Model Parameters for Single Breakthrough Curves

Temp. (K)	Pres. (bar)	k_f (m/s)	D_p (sm^2/s)
338	130	1.736×10^{-5}	9.941×10^{-10}
	120	1.341×10^{-4}	3.907×10^{-9}
	110	1.752×10^{-4}	4.465×10^{-9}
328	130	6.201×10^{-5}	2.835×10^{-9}
	120	9.538×10^{-5}	3.377×10^{-9}
	110	1.657×10^{-4}	3.898×10^{-9}
318	130	7.025×10^{-5}	2.155×10^{-9}
	110	2.825×10^{-5}	2.791×10^{-9}
	100	3.251×10^{-5}	3.310×10^{-9}

Conclusions

Experimental frontal breakthrough curves were obtained for a range of operating conditions. Pressure between 100–130 bar, temperature between 313–328 K, and a three-parameter model were employed to successfully fit the curves.

For identical experimental conditions as above, single breakthrough data were obtained and simulated using the same model. The parameters were in close agreement with those for the frontal curves.

From the frontal breakthrough analysis, the adsorption equilibrium data was modeled by the Langmuir isotherm. The desorption isotherms for this system were consequently found to be unfavorable. The discussion of the desorption isotherms and modeling dynamics for this system will be presented in a forthcoming publication.

Acknowledgments

The authors wish to extend their grateful acknowledgments and appreciation to the National University of Singapore for funding this project through the Academic Research Fund (RP 940647).

Notation

b = Langmuir equilibrium parameter, $m^3/kmol$
C = fluid-phase concentration of adsorbate, $kmol/m^3$ or kg
C_f = ethyl benzene concentration in the bulk supercritical phase, $kmol/m^3$
C_{fi} = ethyl benzene concentration in the bulk supercritical phase at the inlet of packed bed, $kmol/m^3$
C_{fo} = ethyl benzene concentration in the bulk supercritical phase at the beginning of each sorption step (frontal or single), $kmol/m^3$
C_o = maximum fluid-phase concentration of adsorbate for frontal or single breakthrough analysis, $kmol/m^3$ or kg
$\overline{C}_{po}$ = average ethyl benzene concentration in the pores at the beginning of each sorption step (frontal or single), $kmol/m^3$
D_{AB} = binary diffusion coefficient, m^2/s
D_f = bulk diffusivity of ethyl benzene in supercritical CO_2, m^2/s
D_p = effective pore diffusivity of ethyl benzene in supercritical CO_2, m^2/s
D_s = surface diffusivity of ethyl benzene, m^2/s
k_p = overall pore mass-transfer coefficient, m/s
P_r = reduced pressure, P/P_c
q_s = adsorption capacity of adsorbent, kmol/kg
q^* = equilibrium adsorbed phase sorbate concentration, kmol/kg
$\overline{q}$ = adsorbed phase sorbate concentration, kmol/kg
$\overline{q_o}$ = adsorbed phase sorbate concentration at the beginning of each sorption step (frontal or single), kmol/kg
r = radial coordinate for particle
Sh = Sherwood number
t = time, s
T_c = critical temperature, K
T_r = reduced temperature, T/T_c
u = fluid superficial velocity at supercritical conditions, m/s
z = length along the fixed bed, m
μ = viscosity of CO_2 at supercritical conditions, kg/m·s

Literature Cited

Chimowitz, E. H., and K. J. Pennisi, "Process Synthesis Concepts for Supercritical Gas Extraction in the Crossover Region," *AIChE J.*, **32**, 1665 (1986).

Do, D. D., and R. G. Rice, "Validity of the Parabolic Profile Assumption in Adsorption Studies," *AIChE J.*, **32**, 149 (1986).

Erkey, C., G. Madras, M. Orejuela, and A. Akgerman, "Supercritical Carbon Dioxide Extraction of Organics from Soil," *Environ. Sci. Tech.*, **27**, 1225 (1993).

Kander, R. G., and M. E. Paulaitis, "The Adsorption of Phenol from Dense Carbon Dioxide onto Activated Carbon," *Chemical Engineering at Supercritical Fluid Conditions*, M. E. Paulaitis, J. Penninger, R. Gray, and P. Davidson, eds., Ann Arbor Science, Ann Arbor, MI, p. 461 (1983).

Macnaughton, S. J., and N. R. Foster, "Supercritical Adsorption and Desorption Behavior of DDT on Activated Carbon Using Carbon Dioxide," *Ind. Eng. Chem. Res.*, **34**, 275 (1995).

Neretnieks, I., "Analysis of Some Adsorption Experiments with Activated Carbon," *Chem. Eng. Sci.*, **31**, 1029 (1976).

Porto Jefferson, S., K. Tanida, Y. Sato, S. Takishima, and H. Masuoka, "Adsorption Dynamics of Benzene on Activated Carbon in the Presence of Supercritical Carbon Dioxide," *J. Chem. Eng. Jpn.*, **28**, 388 (1995).

Recasens, F., B. J. McCoy, and J. M. Smith, "Desorption Processes: Supercritical Fluid Regeneration of Activated Carbon," *AIChE J.*, **35**, 951 (1989).

Reid, R. C., J. M. Prausnitz, and B. E. Poling, *The Properties of Gases and Liquids*, 4th ed., McGraw-Hill, New York (1987).

Reverchon, E., "Supercritical Desorption of Limonene and Linalool from Silica Gel: Experiments and Modeling," *Chem. Eng. Sci.*, **52**, 1019 (1997).

Ruthven, D. M., *Principles of Adsorption and Adsorption Processes*, Wiley, New York (1984).

Seidel, A., and P. S. Carl, "The Concentration Dependence of Surface Diffusion for Adsorption on Energetically Heterogeneous Adsorbents," *Chem. Eng. Sci.*, **44**, 189 (1989).

Shoijbara, H., Y. Sato, S. Takishima, and H. Masuoka, "Adsorption Equilibria of Benzene on Activated Carbon in the Presence of Supercritical Carbon Dioxide," *J. Chem. Eng. Jpn.*, **28**, 245 (1995).

Tan, C. S., and D. C. Liou, "Desorption of Ethyl Acetate from Activated Carbon by Supercritical Carbon Dioxide," *Ind. Eng. Chem. Res.*, **27**, 988 (1988).

Villadsen, J., and M. L. Michelsen, *Solution of Differential Equation Models by Polynomial Approximation*, Prentice-Hall, Englewood Cliffs, NJ (1978).

Wakao, N., and S. Kaguei, *Heat and Mass Transfer in Packed Beds*, Gordon and Breach, New York (1982).

Manuscript received Mar. 4, 1998, and revision received June 16, 1998.